A Novel Mode Un-Mixing Approach in Variational Mode Decomposition for Fault Detection in Wound Rotor Induction Machines

Reza Bazghandi [1], Mohammad Hoseintabar Marzebali [1] , Vahid Abolghasemi [2] and Shahin Hedayati Kia [3,*]

[1] Department of Electrical Engineering and Robotic, Shahrood University of Technology, Shahrood 36199-95161, Iran; r.bazghandi@shahroodut.ac.ir (R.B.); m.hoseintabar@shahroodut.ac.ir (M.H.M.)
[2] School of Computer Science and Electronic Engineering, University of Essex, Colchester CO4 3SQ, UK; v.abolghasemi@essex.ac.uk
[3] Laboratory MIS UR4290, University of Picardie "Jules Verne", 33 rue St Leu, 80039 Amiens, France
* Correspondence: shdkia@u-picardie.fr

Abstract: Condition monitoring of induction machines (IMs) with the aim of increasing the machine's lifetime, improving the efficiency and reducing the maintenance cost is necessary and inevitable. Among different types of methods presented for mechanical and electrical fault tracing in induction machines, stator current signature analysis has attracted great attention in recent decades. This popularity is mainly due to the non-invasive nature of this technique. A non-recursive method named variational mode decomposition (VMD) is used for the decomposition of any signal into several intrinsic mode functions (IMFs). This technique can be employed for detection of faulty components in a current signature. However, mode mixing of extracted IMFs makes the mechanical and electrical fault detection of IMs complicated, especially in the case where fault indices emerge close to the supply frequency. To achieve this, we rectify the signal of stator current prior to applying VMD. The main advantage of the presented approach is allowing the fault indices to be properly demodulated from the main frequency to avoid mode mixing phenomenon. The method shows that the dominant frequencies of the current signal can be isolated in each IMFs, appropriately. The proposed strategy is validated to detect the rotor asymmetric fault (RAF) in a wound rotor induction machine (WRIM), in both transient and steady-state conditions.

1. Introduction

Induction machines (IMs) are one of the most important components in modern industry. The utilization of induction machines with all capacities in different industries has been confirmed [1]. On the other hand, IMs have significant advantages over synchronous and DC machines, such as lower cost, simplicity and robustness [2]. Due to the operator's safety and the widespread use of this type of machine in several industries, condition monitoring and fault diagnosis in IMs are very important and inevitable [3–6]. Generally, IMs are one of the industry bases, and the use of these machines is necessary for many factories. Numerous surveys have shown that bearing and insulation losses are the most typical failures in IMs, whereas rotor faults usually account for 15–20% depending on the survey. One of the faults in IMs is asymmetry rotor fault, caused by different factors [7]. This type of fault usually happens due to broken rotor bars (BRBs) or brief junction of the rotor windings in wound rotor induction machines (WRIMs). Several approaches have been proposed in recent years to detect faults and improve reliability of the IMs. Despite many methods and strategies presented in the past, many factories and businesses face unexpected failures. Numerous commercial products that use low-to-medium power

IMs are characterized by non-cost-effectiveness [8]. Many sensors can collect signals and data for condition monitoring of IMs and fault detection. These sensors can measure various parameters such as voltage [9] and current [10–12], stray flux [13,14], singular value decomposition of the stator current [15], load torque analysis [16], neural network-based detection [17], etc. Some of these methods are invasive and rarely noticed. On the other hand, some strategies based on non-invasive measurements are superior to the different existing strategies. One of these non-invasive methods is the motor current signature analysis (MCSA), which measures the current of one or more stator phases [18]. MCSA strategy requires a frequency analysis such as fast Fourier transform (FFT) in steady-state mode [19]. For some applications such as wind turbines, electric vehicles or any industrial process that uses variable speed drives, IMs operate under continuous speed and load changes, and faults in these applications often occur under transient conditions. Therefore, FFT-base analysis is not found helpful. Alternatively, advanced signal processing strategies such as wavelet transform [20], short-time Fourier transform (STFT), Wigner–Will transform, or synchro-squeezing wavelet transform (WSST) should be employed [21,22].

Recently, the VMD technique along with deep learning methods was used to classify the healthy and faulty states of machines [23]. VMD technique is used to decompose the input signal into different intrinsic mode functions (IMFs) where each IMFs has a dominant frequency. In this case, if the effects of two dominant frequencies emerge close to each other, separation and isolation of these two effects cannot be carried out properly [24–26]. Therefore, in the no-load condition (low slips) in which the RAF characteristic frequency appears close to the supply frequency, the detection of faults in the electrical signature, where RAF modulates with supply frequency, is complicated. Generally, the VMD techniques are used for fault diagnosis in vibration signals of machines and improved by optimization of its parameters [27]. In [28], the detection of inter-turn fault in doubly fed induction machine was investigated based on the VMD technique. VMD was used as a denoising technique. The best IMF was selected based on correlativity coefficient, kurtosis index and multi-scale permutation entropy and then the reconstructed leakage flux was analyzed through the Hilbert–Hung transform. The zero-sequence voltage component was decomposed to a set of IMFs where the IMF related to the fault was selected for analyzing faults in [29]. The results were only supported by simulation and the effects of mode mixing and detection of fault in low slip was not investigated. A VMD-based notch filter along with Pearson correlation was introduced to find the best IMF related to the fault. The method was compared with the empirical mode decomposition method, and it has been shown that it can be considered for bearing fault detection [30]. However, the effects of mode mixing in the signature of machine in stator current signature analysis for mechanical and electrical faults detection were not studied. Due to the presence of mode mixing in the VMD method, the use of this technique individually cannot decompose the fault signal appropriately, and it is not possible to detect the asymmetric fault using the decomposition signals. Therefore, a strong demodulation method with low computing power is needed. Additionally, the presented demodulation method should be able to solve mode mixing in the VMD technique.

Rotor asymmetry faults (RAF) occur at the frequency of $(1 - 2s)f_s$ which emerge close to the supply frequency (f_s). Since VMD method decomposes the dominant frequencies of the signal to the different IMFs, proximity of RAF index and supply frequency leads to mode mixing phenomenon in the spectrum of extracted IMFs. Therefore, finding the best IMFs would be challenging. In this regard, separation and isolation of these two dominant frequencies leads to prevention of mode mixing in the spectrum of decomposed signals. In this paper, the pre-processed signal of the stator current signature is used in the VMD technique to isolate and separate the dominant frequencies of the stator current spectrum. To address this issue, a new approach based on the VMD of the rectified stator current is introduced for mechanical and electrical fault detection in IMs in steady-state and transient conditions. It is necessary to note that different methods for finding the best IMF have been introduced in recent years, such as frequency band entropy [31]. However, the goal of this

paper is not to find the best IMF, rather to construct an IMF which has minimum mode mixing with the dominant frequency of faults with simple pre-processing method. In brief, our contributions are:

- Studying the effects of mode mixing in the stator's signature with electrical faults for the first time.
- Combining demodulated technique as pre-processing method with VMD to avoid mode mixing of fault characteristic frequency with the dominant frequency.
- Classification of faults through the presented method based on the energy of IMFs obtained through pre-processing and VMD technique.

2. Rectified Stator Current Used as Simplified Demodulation Technique

An asymmetry fault such as broken rotor bars or an asymmetry between the rotor resistances causes an amplitude modulation with a specific frequency in the stator current of induction motors [32].

$$f_{AF} = 2\zeta s f_s \, , \, \zeta = 1, 2, 3, \cdots \tag{1}$$

where f_s and s are the fundamental frequency and slip ratio of the motor, respectively. From the asymmetric fault index mentioned above, the stator phase current of IM in the presence of RAF can be obtained by (2).

$$i_{AF}(t) = I_s cos(2\pi f_s t)[1 + \beta cos(2\pi f_{AF} t)] \tag{2}$$

In (2), β is the severity of the fault expressed by (3) for broken rotor bar fault.

$$\beta \approx \frac{\eta_F}{N_b} \tag{3}$$

According to the main harmonic of the fault and (2), the mathematical equation for motor stator current in the presence of RAF can be written as:

$$i_{AF}(t) = I_s cos(2\pi f_s t) + \frac{\beta}{2}[I_s cos(2\pi(1-2s)f_s t) + I_s cos(2\pi(1+2s)f_s t)] \tag{4}$$

As mentioned, RAF usually appears as broken rotor bars and asymmetric resistance in squirrel cage motors and WRIM. This type of fault causes amplitude modulation in the stator current signal. It is problematic to determine the fault index from the main signal due to the leakage of the main component. Therefore, an efficient and straightforward strategy needs to be introduced to demodulate the fault index from the main harmonic. One of the powerful methods for demodulation is the stator current rectification. By rectifying the stator current, the fault index is well separated from the main component and the fault can be detected correctly. The rectified value of the signal can be simply obtained by taking the corresponding absolute value in theory, and by using a diode bridge in practice:

$$|i_{AF}(t)| = i_{AF}(t) \times sgn(cos(2\pi f_s t)) \tag{5}$$

where

$$sgn(x) = \begin{cases} 1 & x > 0 \\ 0 & x = 0 \\ -1 & x < 0 \end{cases} \tag{6}$$

Generally, the $sgn(cos(2\pi f_s t)$ term, produces a square wave and can be extended as the following series:

$$sgn(cos(2\pi f_s t)) = \frac{4}{\pi} \sum_{n=1,3,5,\cdots}^{+\infty} \frac{sin(\frac{n\pi}{2})}{n} cos(2n\pi f_s t) \tag{7}$$

Now by combining (4), (5), (6) and (7), the final equation for the rectified signal of the IMs can be obtained as follows:

$$|i_{AF}(t)| = \frac{4I_s}{\pi}(\frac{1}{2} + \frac{\beta}{2}cos(2\pi(2sf_st)+$$

$$\sum_{n=3,5,...}^{+\infty}(\frac{sin(\frac{n\pi}{2})}{n}cos(2n\pi f_st) \times cos(2\pi f_st) + \frac{\beta}{2}cos(2\pi f_s(1 \pm 2s)t)) \tag{8}$$

As can be seen in (8), the rectified stator current of IMs consists of three terms: the DC component, a low-frequency part where the frequency is equal to the fundamental RAF harmonic and a set of harmonics with higher harmonics of faults and fundamental supply frequency.

3. Variation Mode Decomposition

In the late 1990s, Huang introduced an algorithm for the recursive decomposition of a signal into different unknown modes called Empirical Mode Decomposition (EMD). Despite the heavy mathematical equations and some apparent shortcomings, the EMD method is used in many time–frequency applications such as bearing faults [33–35]. Then, in 2013, a practical technique called Variational Mode Decomposition (VMD) was presented by Dragomiretskiy and Zosso [36].

In contrast to the EMD, VMD works based on a fully non-recursive decomposition model where all modes are extracted at one step. This model aims to obtain a set of related central modes and frequencies so by the sum of all modes reconstructs the input signal. The signals decomposed by this method are called IMFs. The methods based on EMD have the following limitations: (1) Their responses are sensitive to noise. (2) Reversible screening, which is present in most strategies, does not permit backward error correction. (3) There is a hard frequency band limitation in wavelet-based methods. Therefore, the VMD technique has been introduced to address these limitations. Next, we explain some necessary concepts in signal processing followed by VMD's mathematics.

3.1. Wiener Filtering

The simple problem of noise reduction is defined as follows. The observed signal $y_0(t)$ is the sum of the main signal $y(t)$ with a Gaussian noise λ with a mean of zero.

$$y_0(t) = y(t) + \lambda \tag{9}$$

$y(t)$ is the clean signal which should be recovered where (9) is a typical ill-posed inverse problem [24,25]. It is defined in the classical method using Tikhonov tuning.

$$\min_{y}\{||y - y_0||_2^2 + \alpha||\partial_t y||_2^2\} \tag{10}$$

where α denotes the variance of the white noise. The above equation can be associated with Euler–Lagrange equations and is usually solved by Fourier transform.

$$\hat{y}(\omega) = \frac{\hat{y}_0}{1 + \alpha\omega^2} \tag{11}$$

where $\hat{y}(\omega) := F\{y(\cdot)\}(\omega) := \frac{1}{\sqrt{2\pi}}\int_R y(t)e^{-j\omega t}\,dt$ with $j^2 = -1$ is the Fourier transform of $y(t)$. It is clear that the recovered signal $y(t)$ is a low-pass narrow-band selection of the original signal $y_0(t)$ near $\omega = 0$. In fact, by convolution (11) with Wiener filter, the solution has been obtained, and the signal has a low-pass spectral range of $\frac{1}{\omega^2}$ [24].

3.2. Hilbert Transform and Analytic Signal

In mathematics and signal processing, a linear, shift-invariant operator that maps all cosine functions into corresponding sine functions is called the Hilbert transform. The 1-D Hilbert transform is an all-pass filter characterized by the following transfer function.

$$\hat{h}(\omega) = -j \cdot sgn(\omega) = \frac{-j\omega}{|\omega|} \tag{12}$$

This linear operator is a multiplier operator in the frequency domain with an impulse response $h(t) = \frac{1}{\pi t}$. Since the result of convolution is not integrable, the Hilbert transform of a $y(t)$ is acquired as the Cauchy principal value of the convolution integral:

$$H(y(t)) = \frac{1}{\pi} p.v. \int \frac{y(v)}{t - v} \, dv \tag{13}$$

The most prominent application of the Hilbert transform is to construct an analytical signal from a purely real signal. If $y(t)$ is assumed to be a purely real signal, then the complex-valued analytic signal is now defined as:

$$y_A(t) = y(t) + jH(y(t)) = A(t)e^{j\phi t} \tag{14}$$

3.3. Frequency Mixing and Heterodyne Demodulation

When two signals are combined in a non-linear fashion, it is called mixing. Thus, the cross-frequency is visible at the output. The simplest type of mixing is the multiplication of two signals. Multiplication of two real signals with the frequencies ω_1 and ω_2 produces two frequencies $\omega_1 - \omega_2$ and $\omega_1 + \omega_2$ at the output respectively, as illustrated by the following trigonometric identity:

$$2 \cdot cos(\omega_1 t)cos(\omega_2 t) = cos((\omega_1 + \omega_2)t) + cos((\omega_1 - \omega_2)t) \tag{15}$$

The mixing of the above analytical signals is:

$$e^{j\omega_1 t}e^{j\omega_2 t} = e^{j(\omega_1 + \omega_2)t} \tag{16}$$

The output signal is a single frequency signal. With the help of properties, the analysis of the analytical signal is:

$$f_A(t)e^{-j\omega_0 t} \longleftrightarrow \hat{f}_A(\omega) * \delta(\omega + \omega_0) = \hat{f}_A(\omega + \omega_0) \tag{17}$$

where δ and $*$ represent the Dirac distribution and convolution operator, respectively. The product of a synthetic signal with a pure exponential signal is simple frequency shifting [29].

3.4. Theory of VMD

The main purpose of this technique (VMD) is to decompose and break down a real valued input signal into the discrete number of IMFs. In addition to reproducing the input signal, it also has specific sparsity properties. Here, the sparsity prior to each mode is selected as the bandwidth of that mode. In other words, it is assumed that each mode k is more compressed around the central pulsation ω_k. This central frequency is to be determined along with the decomposition. The following steps are performed to determine the bandwidth of each mode. For each mode, calculate the similar synthetic signal using the Hilbert transform to obtain a unilateral frequency spectrum. For each mode, the frequency spectrum of the mode is shift to the "base-band" by mixing with a single-frequency signal

with a frequency of ω_k (demodulation step). With the help of bandwidth by Gaussian function H, the demodulated signal is extracted. The result is obtained as follows:

$$\min_{\{u_k\}\{\omega_k\}} \left\{ \sum_k ||\partial_t \left[\left(\delta(t) + \frac{j}{\pi t} \right) * u_k(t) \right] e^{-j\omega_k t}||_2^2 \right\}$$

$$s.t. \sum_k u_k = f \qquad (18)$$

where $u_k = u_1, \cdots, u_k$ and $\omega_k = \omega_1, \cdots, \omega_k$ are the abbreviated representations set of all modes and their center frequencies, respectively. $\sum_k := \sum_{k=1}^k$ denotes the sum of all modes. The reconstruction signal constraint can be applied to the optimization problem differently. Here, both the quadratic penalty terms and Lagrange multipliers are used to transform the problem into a new unconstrained optimization problem. Combining these two terms produces nice convergence properties of the quadratic penalty at finite weight and the strict enforcement of the constraint by the Lagrangian multiplier. As a result, the main optimization problem (18) becomes the following equation:

$$L(u_k, \omega_k, \lambda) := \alpha \sum_k ||\partial_t \left[\left(\delta(t) + \frac{j}{\pi t} \right) * u_k(t) \right] e^{-j\omega_k t}||_2^2$$

$$+ ||f(t) - \sum_k u_k(t)||_2^2 + \langle \lambda(t), f(t) - \sum_k u_k(t) \rangle \qquad (19)$$

The saddle point of the above Equation (19) which is obtained from iterative sub-optimization called alternate direction method of multipliers (ADMM) is the answer of Equation (18). To find the answer, the following two algorithms (Algorithms 1 and 2) can be used [29].

Algorithm 1 Complete optimization of VMD

Initialize $\qquad \{u_k^1\}, \{\omega_k^1\}, \lambda^1, n \leftarrow 0$
Repeat $\qquad n \leftarrow n + 1$

  for k=1:K **do**

    Update u_k:

    $u_k^{n+1} \leftarrow \underset{u_k}{argmin} \quad \mathscr{L}(\{u_{i<k}^{n+1}\}, \{u_{i \geq k}^n\}, \{\omega_i^n\}, \lambda^n)$

  end for

  for k=1:K **do**

    Update ω_k:

    $\omega_k^{n+1} \leftarrow \underset{\omega_k}{argmin} \quad \mathscr{L}(\{u_i^{n+1}\}, \{\omega_{i<k}^{n+1}\}, \{\omega_{i \geq k}^n\}, \lambda^n)$

  end for

  Dual ascent:

  $\lambda^{n+1} \leftarrow \lambda^n + \tau(f - \sum_k u_k^{n+1})$

  Until convergence: $\sum_k ||u_k^{n+1} - u_k^n||_2^2 / ||u_k^n||_2^2 < \epsilon$

After optimization of the above algorithm, a complete algorithm is obtained for VMD method (Algorithm 2).

Algorithm 2 Complete optimization of VMD

Initialize $\{\hat{u}_k^1\}, \{\omega_k^1\}, \hat{\lambda}^1, n \leftarrow 0$
Repeat $n \leftarrow n+1$

for k=1:K **do**

     Update $\hat{u}_k$ for all $\omega \geq 0$:

$$\hat{u}_k^{n+1}(\omega) \leftarrow \frac{\hat{f}(\omega) - \sum_{i<k} \hat{u}_i^{n+1}(\omega) - \sum_{i>k} \hat{u}_i^n(\omega) + \frac{\hat{\lambda}^n(\omega)}{2}}{1 + 2\alpha(\omega - \omega_k^n)^2}$$

     Update ω_k
$$\omega_k^{n+1} \leftarrow \frac{\int_0^\infty \omega |\hat{u}_k^{n+1}(\omega)|^2 d\omega}{\int_0^\infty |\hat{u}_k^{n+1}(\omega)|^2 d\omega}$$
end for

Dual ascent for all $\omega \geq 0$:

$$\hat{\lambda}^{n+1}(\omega) \leftarrow \hat{\lambda}^n(\omega) + \tau\left(\hat{f}(\omega) - \sum_k \hat{u}_k^{n+1}(\omega)\right)$$

Until convergence: $\sum_k ||\hat{u}_k^{n+1} - \hat{u}_k^n||_2^2 / ||\hat{u}_k^n||_2^2 < \epsilon$

All IMFs are obtained from the above algorithm, and we can analyze them.

4. Flowchart of the Proposed Method

The rectification of stator current, proposed above, demodulates the RAF characteristic frequency from the supply frequency. Consequently, RAF index can be detected in the frequency of $2sf_s$ close to the frequency of DC value. As a result, separation of modes can be well carried out by using rectified signal of stator current as a pre-processing stage of the proposed technique. In fact, the goal of this study is to separate the supply frequency from RAF index. In this regard, the demodulation technique needs to be used to isolate and separate these two dominant frequencies in the spectrum of stator current. Among different demodulation techniques, rectified stator current is simple and can be implemented easily. The flowchart of the proposed technique is shown in Figure 1 in which at first the stator current samples of WRIM are obtained through three-phase current sensor with frequency of 2 kHz for 12 s and then the considered signal is rectified by means of sign function. In the next step, the rectified stator current is decomposed to five IMFs. The specific IMF, in which the RAF characteristic frequency is a dominant frequency, is selected for spectrum analyses in steady-state and transient conditions by means of FFT and synchro-squeezing transform (WSST), respectively.
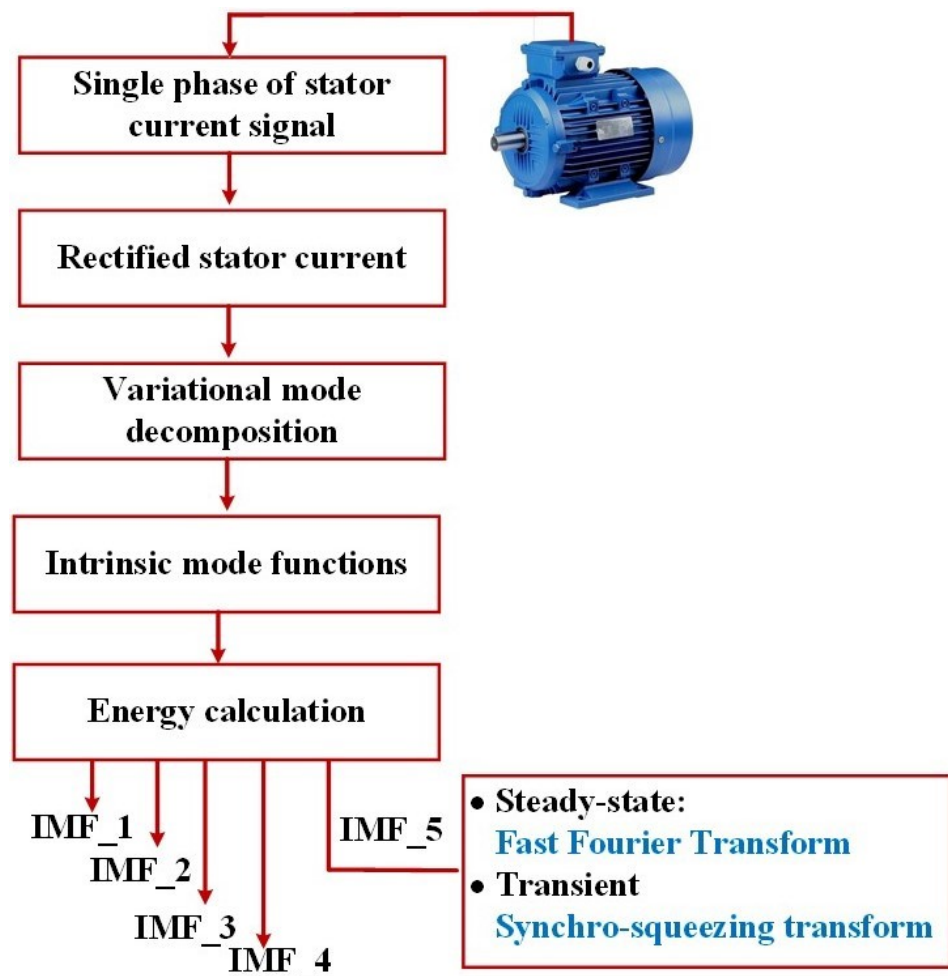
Figure 1. Flowchart of proposed technique.

5. Experiments and Results

This section tests the proposed method on a WRIM in both steady-state and transient conditions. After rectifying the stator current, the obtained signal is analyzed by the VMD method and then the fault index can be detected in both steady-state and transient modes. By short-circuit the rotor windings of the induction motor, one of the phase resistances gradually increase from other phases and an asymmetric fault occurs in WRIM. In this paper, by applying an external resistance to the rotor windings, an asymmetric fault can be created in the WRIM, and then the motor can be analyzed (Figure 2). The parameters of the studied WRIM are presented in Table 1.
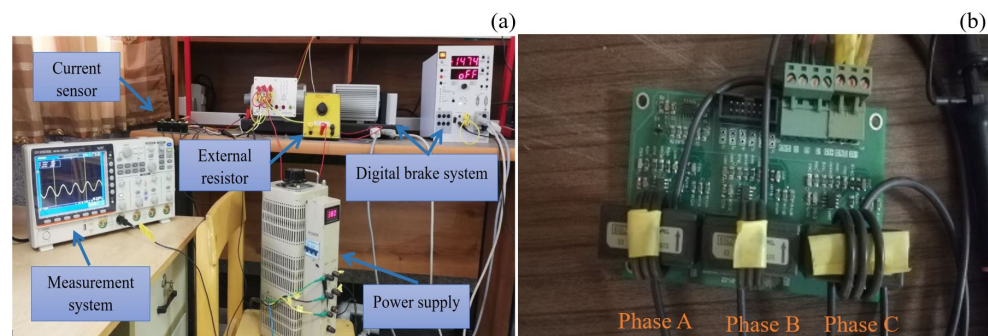

Figure 2. (**a**) Experimental setup. (**b**) current sensor.

Table 1. Specification of WRIM used for condition monitoring process.

Parameters	Value
Rated power (W)	370
Nominal voltage (V)	380
Number of poles	4
Impedance (Ω)	5
Synchronous speed (RPM)	1500
Supply frequency (Hz)	50

The proposed method is verified under different operational points. In this regard, the proposed technique has been investigated in transient and steady-state conditions. All the tests have been carried out in the laboratory of Shahrood University of Technology. The current samples are recorded by the current sensor and the oscilloscope. The type of current sensor used in this experiment is Hall Effect Current Sensor given in S25P100D15X from Tamura. The digital braking system is used to implement transient mode. By applying torque, this system is able to increase or decrease the speed of the motor, which has finally caused a transient condition in the system. In steady-state conditions, the stator current has been recorded through a three-phase current sensor with sampling frequency of 2 kHz. However, in the transient condition two operational modes are selected based on deceleration and acceleration conditions. It is necessary to note that, in the majority of papers, the methods were tested from start-up to a nominal speed condition where the slip of the machine changes from $s = 1$ to value close to zero. In reality, the machine operates close to the nominal operational point. Therefore, in this paper, the proposed method in transient conditions is tested under slight variations in the slip of machine close to the nominal slip of the machine.

5.1. Steady-State Condition

In this section, at first, the stator current signal under RAF is verified through the VMD technique without a pre-processing stage. The stator current signal is extracted for 12 s with a sampling frequency of 2 kHz. The IMFs of the extracted signal are shown in Figure 3a,c. Based on the equations of the VMD technique, the signal decomposition will be continued until the equation $\sum_k ||\hat{u}_k^{n+1} - \hat{u}_k^n||_2^2 / ||\hat{u}_k^n||_2^2 < \epsilon$ which is found in the Algorithm 2 convergence. Regarding this fault signal that we have here, when we reach the fifth IMF, this equation converges. The VMD technique decomposes the mother signal to the five IMFs. Then, the stator current is pre-processed by the rectification stage. The extracted IMFs are shown in Figure 3b,d.
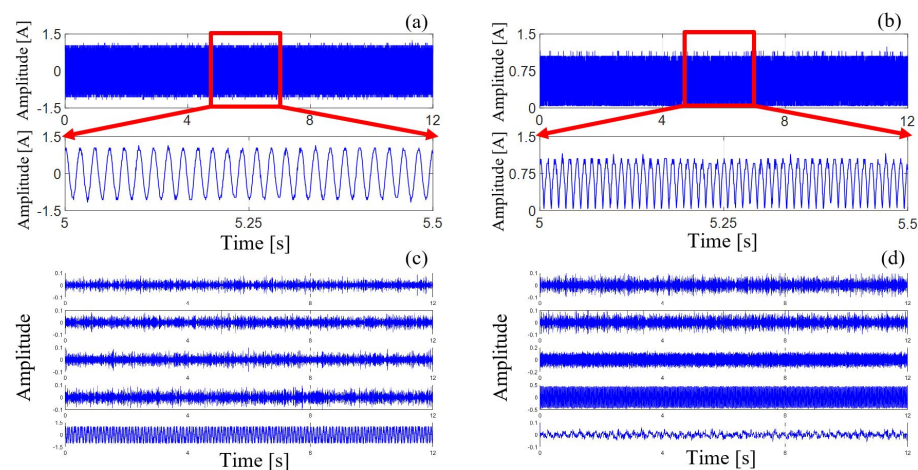

Figure 3. Signals and IMFs were obtained from the VMD (**a**) Stator current signal. (**b**) Rectified stator current signal. (**c**) IMFs are obtained from main signals. (**d**) IMFs are obtained from rectified signals.

In order to investigate the impacts of fault on current spectrum of IM, Fast Fourier transform of each IMFs are given. It can be observed that the amplitude of the fault is severely affected by the amplitude of dominant supply frequency and mode mixing phenomena (Figure 4). It can be found out that the amplitude of fault characteristic frequency in the 5th IMF has higher value in comparison with other IMFs (Figure 4e). The amplitudes of fault characteristic frequencies while the dominant frequency is eliminated in the first four IMFs are very low (Figure 4a–d). Therefore, it is difficult to detect faults in the first four IMFs due to attenuation of the fault index. On the other hand, the phenomenon of mode mixing between two dominant frequencies (supply frequency and fault characteristic frequency) is obvious where both frequencies can be detected (Figure 4e). Therefore, fault detection based on the energy of the 5th IMF cannot be considered due to mode mixing issue. To address this problem, in this paper the VMD technique is combined with a rectification pre-processing stage. The obtained results show that the amplitudes of fault characteristic frequency have higher values in the first four IMFs in comparison with the previous case (Figure 5a–d). However, the major difference occurs in 5th IMF, where the supply frequency effect is eliminated (Figure 5e). As shown in Figure 5e, the fault index is well demodulated and detected from the main component. The last IMF (5th IMF) has the highest fault severity -53 dB after testing on all IMFs. The fault frequency in the 5th IMF for normal mode (without rectification) is equal to 46.08 Hz (Table 2). Although the amplitude of the fault characteristic frequency in 5th IMF is reduced in comparison with the previous case, the mode mixing problem is solved (Table 2). Since in the 5th IMF the dominant frequency of the spectrum is the characteristic frequency of RAF, the energy of the signal can be introduced as fault index for detection of RAF in IMs. In this regard, 50 data points including 12 s with a sampling frequency of 2 kHz are obtained for this purpose in each fault severity and healthy case. The data are collected through a current sensor for three RAF severities which are emulated by external resistances (0.03 p.u. (per unit of rotor resistance), 0.09 p.u. and 0.15 p.u.). The following equation can be used to calculate the energy of the 5th IMF signal (E_{IMF5}).

$$E_{IMF5} = \frac{1}{N} \sqrt{\sum_{i=1}^{N} |x_i|^2} \tag{20}$$

x_i are obtained samples of the 5th IMF of the original stator current signal. In order to investigate the amplitude of fault characteristic frequency, the normalized energy of the 5th IMF signal relative to the original signal (E_0) is considered as criterion for a healthy case and three faulty cases.

$$E_N = \frac{E_{IMF5}}{E_0} \tag{21}$$

The critical issue is how to choose the appropriate IMF for fault detection. The energy of each IMF has been used to achieve this goal. Equations (20) and (21) can be used to calculate the energy of each IMF. The IMF that represents the fault signal has more energy than other IMFs. After calculating the energy of all IMFs, the desired IMF (with the highest energy) is selected, and Fourier transform or WSST technique can be performed on the fault signal (Figure 5).

In each four cases, 50 data points of the stator current are recorded, and the normalized energy of the 5th IMF is calculated. It can be well observed that the introduced fault index can detect RAF in different severities perfectly even in low fault severity (R_{unb} = 0.03 p.u.). R_{unb} is equivalent to dividing the resistance applied to the stator winding by the resistance of the rotor. Here, the resistance of the rotor is 34 Ω and the applied resistance is equal to 1 Ω, which ultimately makes R_{unb} equal to 0.03 p.u. In order to have a better view of the presented normalized energy data of the 5th IMF, the average value of these data is given as single line in Figure 6, colored to fit each case. The average results of this index show that it has a good ability to isolate and detect RAF and its severity.
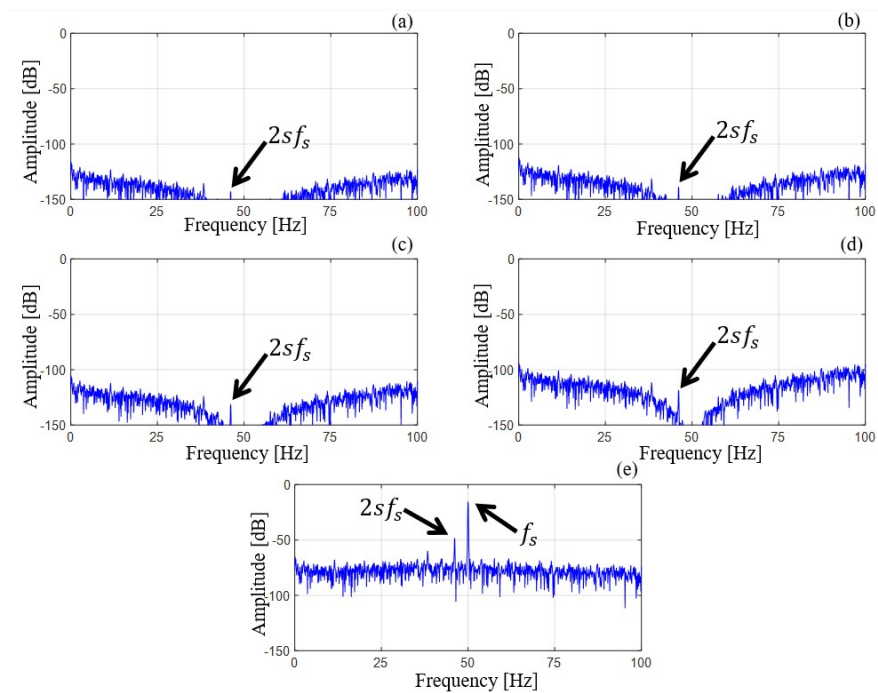
Figure 4. Fourier transform of all IMFs that are obtained from the main current signal (**a**) Fourier transform of first IMF. (**b**) Fourier transform of second IMF. (**c**) Fourier transform of third IMF. (**d**) Fourier transform of 4th IMF. (**e**) Fourier transform of 5th IMF.
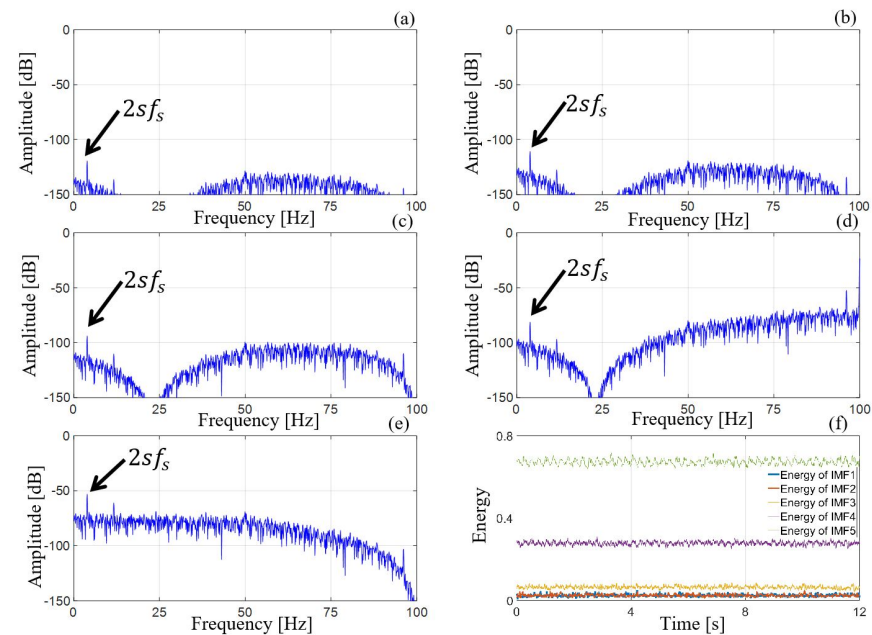

Figure 5. Fourier transform of all IMFs that are obtained from the rectified signal (**a**) Fourier transform of first IMF. (**b**) Fourier transform of second IMF. (**c**) Fourier transform of third IMF. (**d**) Fourier transform of 4th IMF. (**e**) Fourier transform of 5th IMF. (**f**) Energy of all IMFs.

Table 2. Amplitude of RAF index in different IMFs.

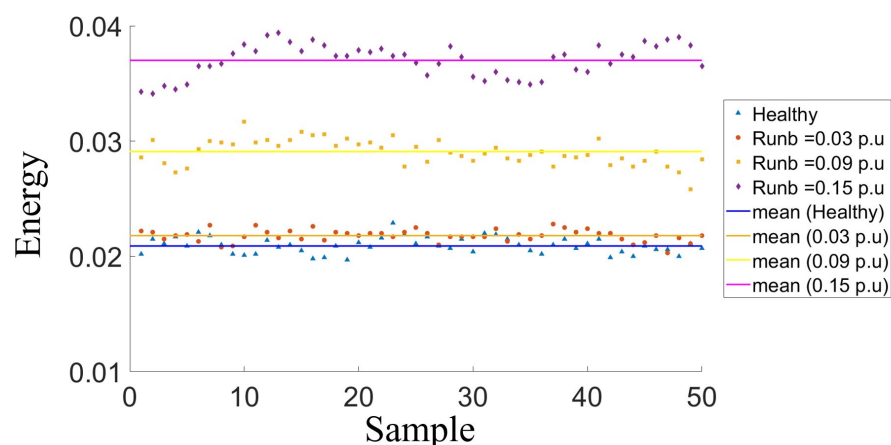|	**IMF1**	**IMF2**	**IMF3**	**IMF4**	**IMF5**
Rectified signal	−119.39 dB	−110.77 dB	−93.92 dB	−81.25 dB	−53.17 dB
Main signal	−142.92 dB	−138.74 dB	−131.32 dB	−118.53 dB	−48.44 dB

Figure 6. Comparison of the energies for the fifth IMF in different modes.

The five IMFs are obtained from the VMD technique can be seen well in Figure 5. The fault index is specified in all five IMFs, but in the fifth IMF, the fault frequency characteristic is observed more strongly. As mentioned, to detect the superior IMF, the energy calculation of the signals can be used. The average energy for the first to fifth IMFs is equal to 0.022, 0.023, 0.065, 0.27 and 0.67, respectively (Figure 5). In Figure 6, the average normalized energy for four states (R_{unb} = 0.03 p.u., R_{unb} = 0.09 p.u., R_{unb} = 0.15 p.u. and healthy) in the fifth IMF in different fault severities is equal to 0.037, 0.029, 0.022 and 0.02, respectively.

5.2. Transient Condition

The proposed technique is evaluated in transient conditions. In this regard, the acceleration and deceleration conditions and their IMFs in two cases of with single VMD and proposed technique are considered (Figures 7 and 8). Previously, in the majority of the papers, the start-up stator current of machine, where the slip of machine varies extensively, is considered. However, in reality, machine slip under normal operation varies slightly. Therefore, in this paper a slight variation in the slip of the machine is used for evaluation of the proposed method (Figure 7a,b). The experimental results show that the pre-processed technique, which is based on rectification of obtained stator current, can avoid the mode mixing process. In order to test this, two methods based on single VMD and proposed methods are compared. It can be observed that, based on the single VMD technique without any pre-processing stage, the amplitude of RAF in the spectrum of the 5th IMF has maximum value in comparison with other IMFs. Detecting a fault index in the presence of the supply frequency is not possible in this case while the pre-processed signal can demodulate the RAF fault from the supply frequency in the 5th IMF (Figure 9a,b).

In this case, the RAF characteristic frequency is the dominant frequency of the 5th IMF and can be well detected in the time-frequency analysis which is carried out by wavelet WSST (Figure 9c,d). By using the WSST technique, a narrow band of time-frequency analysis can be observed. It is worth mentioning that this technique needs to be used for demodulated signal to provide proper distinction between fault index and main frequency. As a result, first the original signal should be demodulated and finally this time-frequency method should be used. The proposed method has been compared with other time-frequency methods, as analyzed in Section 6.
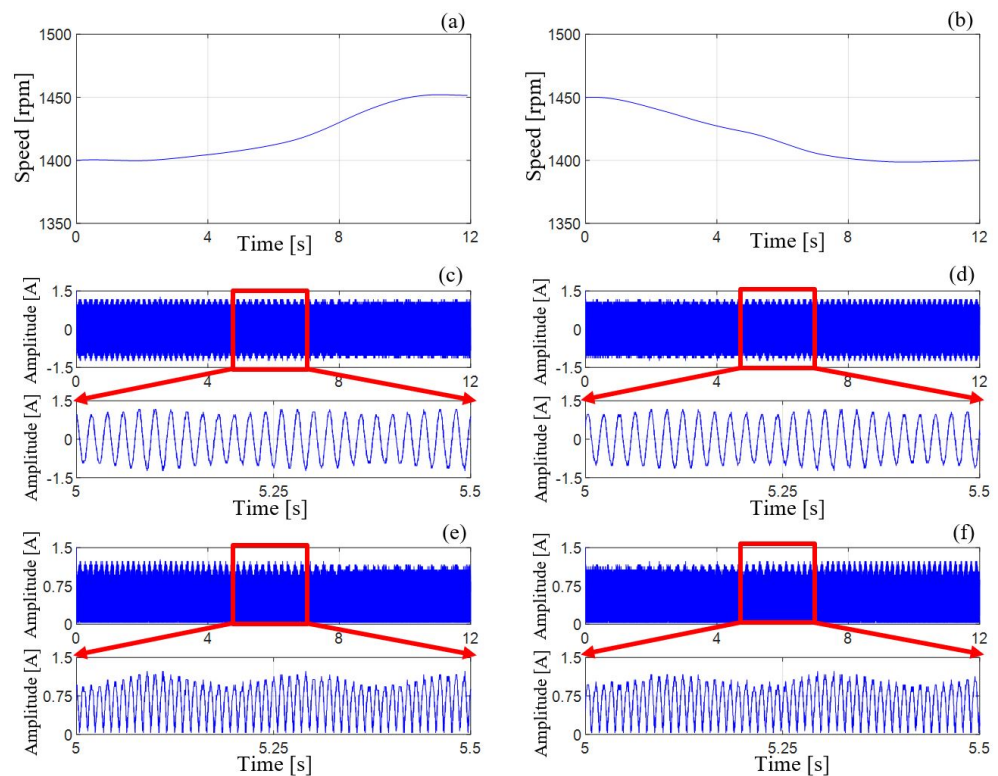
Figure 7. Speed and current signals of motor (**a**) Speed changes in acceleration mode. (**b**) Speed changes in deceleration mode. (**c**) Stator current signal in acceleration mode. (**d**) Stator current signal in deceleration mode. (**e**) Rectified Stator current signal in acceleration mode. (**f**) Rectified Stator current signal in deceleration mode.
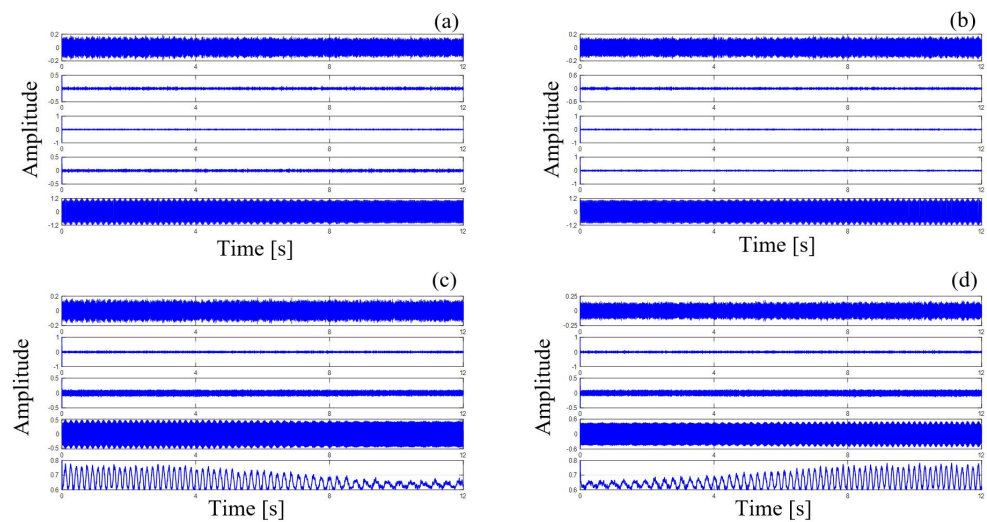

Figure 8. IMFs that are obtained from the main and rectified signals (**a**) Stator current IMFs for acceleration mode. (**b**) Stator current IMFs for deceleration mode. (**c**) Rectified stator current IMFs for acceleration mode. (**d**) Rectified stator current IMFs for deceleration mode.
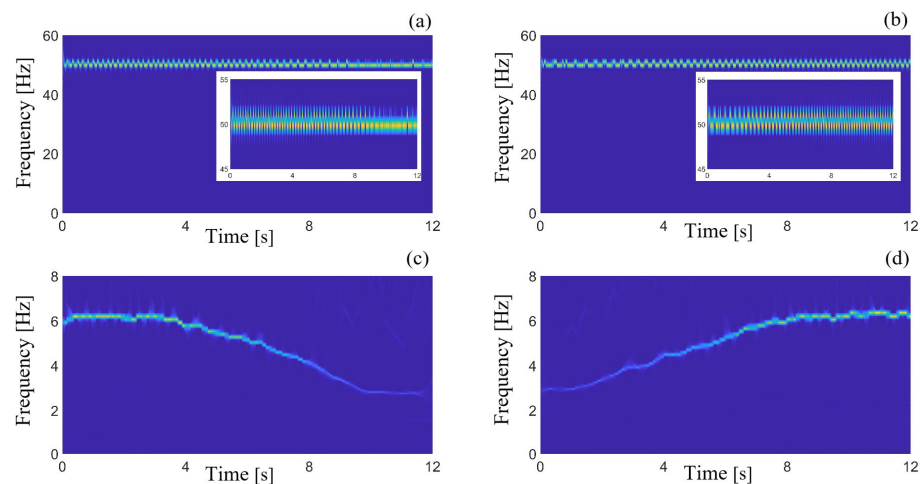
Figure 9. Time-frequency analysis of the IMFs obtained from the VMD (**a**) WSST for main signal (fifth IMF) in acceleration mode. (**b**) WSST for main signal (fifth IMF) in deceleration mode. (**c**) WSST for rectified signal (fifth IMF) in acceleration mode. (**d**) WSST for rectified signal (fifth IMF) in deceleration mode.

6. Comparison between Proposed Technique and Other Approaches

In this section, a practical comparison between the proposed method and other approaches for validating the proposed method is presented. First, the presented demodulation method is compared with the Teager–Kaiser energy operator (TKEO) method, and finally, the WSST technique is compared with other time-frequency methods. According to Figure 10, in the TKEO method, the severity of asymmetric error is lower than the proposed method. Short-time Fourier transform (STFT) technique is used for comparison in time-frequency method. This method is not able to create a narrow band and does not have enough resolution to detect the fault characteristic frequency (Figure 11).
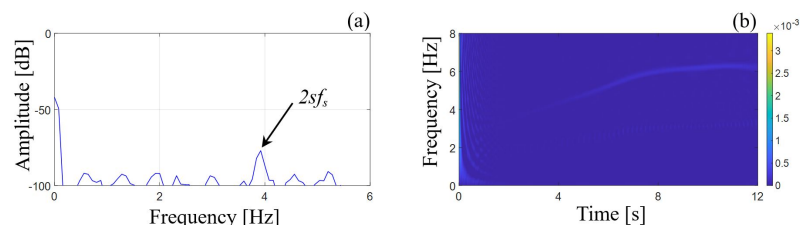

Figure 10. TKEO result (**a**) Steady−state analysis. (**b**) Transient analysis.
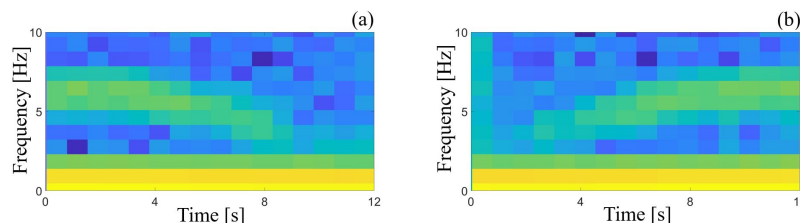

Figure 11. Transient analysis (**a**) STFT for acceleration mode. (**b**) STFT for deceleration mode.

7. Conclusions

This paper presents a new technique based on stator current signature of IMs for electrical and mechanical fault detection. The proposed technique has been tested on a 0.25 kW WRIM. In the proposed method, the rectification technique is used to eliminate the mode mixing and then the VMD method is used to compute the fault index in both steady-state and transient modes. One of the limitations of the proposed technique is the need to calculate the energy of all IMFs to find the best match for fault detection process. In this regard, proper technique for finding the best IMF can be investigated as our future

works in this field of study. In this regard, WSST has been used to compute the fault index in transient mode. Easier practical implementation due to the measurement of the single phase of stator current and rectification process, which can be carried out through simple computational program, ability to separate and demodulate the asymmetric fault index from the main component and elimination of the mode mixing are the advantages of the proposed method.

Author Contributions: Conceptualization, R.B., M.H.M. and V.A.; Methodology, R.B., M.H.M. and V.A.; Software, R.B., M.H.M. and V.A.; Validation, R.B., M.H.M. and V.A.; Formal analysis, R.B., M.H.M. and V.A.; Investigation, R.B., M.H.M. and V.A.; Resources, R.B., M.H.M. and V.A.; Data curation, R.B., M.H.M. and V.A.; Writing—original draft, R.B., M.H.M. and V.A.; Writing—review & editing, R.B., M.H.M., V.A. and S.H.K.; Visualization, R.B., M.H.M., V.A. and S.H.K.; Supervision, M.H.M., V.A. and S.H.K.; Project administration, M.H.M.; Funding acquisition, M.H.M. All authors have read and agreed to the published version of the manuscript.

Data Availability Statement: Not applicable.

Conflicts of Interest: The authors declare no conflict of interest.

Abbreviations

The following abbreviations are used in this manuscript:

f_s	Supply frequency
s	Slip ratio
f_{Af}	Asymmetric fault frequency
ζ	Harmonic Order
i_{Af}	Asymmetric fault current
I_s	Maximum current
β	Modulation index
η_f	Numeral of broken rotor bars
N_b	Numeral of rotor bars of the induction motor
$y(t)$	Clean signal
N	Length of signal
E_{IMF}	Energy of IMF
E_N	Normalized energy
∂_t	Partial derivative

References

1. Halder, S.; Bhat, S.; Zychma, D.; Sowa, P. Broken Rotor Bar Fault Diagnosis Techniques Based on Motor Current Signature Analysis for Induction Motor—A Review. *Energies* **2022**, *15*, 8569. [CrossRef]
2. Antonino-Daviu, J.A.; Quijano-López, A.; Rubbiolo, M.; Climente-Alarcon, V. Advanced analysis of motor currents for the diagnosis of the rotor condition in electric motors operating in mining facilities. *IEEE Trans. Ind. Appl.* **2018**, *54*, 3934–3942. [CrossRef]
3. Huang, J.; Cui, L.; Zhang, J. Novel morphological scale difference filter with application in localization diagnosis of outer raceway defect in rolling bearings. *Mech. Mach. Theory* **2023**, *184*, 105288. [CrossRef]
4. Han, T.; Li, Y.-F. Out-of-distribution detection-assisted trustworthy machinery fault diagnosis approach with uncertainty-aware deep ensembles. *Reliab. Eng. Syst. Saf.* **2022**, *226*, 108648. [CrossRef]
5. Filippetti, F.; Bellini, A.; Capolino, G.-A. Condition monitoring and diagnosis of rotor faults in induction machines: State of art and future perspectives. In Proceedings of the 2013 IEEE Workshop on Electrical Machines Design, Control and Diagnosis (WEMDCD), Paris, France, 11–12 March 2013; pp. 196–209.
6. Marzebali, M.H.; Bazghandi, R.; Abolghasemi, V. Rotor Asymmetries Faults Detection in Induction Machines under the Impacts of Low-Frequency Load Torque Oscillation. *IEEE Trans. Instrum. Meas.* **2022**, *71*, 1–11. [CrossRef]
7. Abolghasemi, V.; Marzebali, M.H.; Ferdowsi, S. Recursive singular spectrum analysis for induction machines unbalanced rotor fault diagnosis. *IEEE Trans. Instrum. Meas.* **2021**, *71*, 1–11. [CrossRef]
8. de Jesús Rangel-Magdaleno, J. Induction machines fault detection: An overview. *IEEE Instrum. Meas. Mag.* **2021**, *24*, 63–71. [CrossRef]

9.   Rajagopalan, S.; Habetler, T.G.; Harley, R.G.; Sebastian, T.; Lequesne, B. Current/voltage-based detection of faults in gears coupled to electric motors. *IEEE Trans. Ind. Appl.* **2006**, *42*, 1412–1420. [CrossRef]

10.   Marzebali, M.H.; Kia, S.H.; Henao, H.; Capolino, G.-A.; Faiz, J. Planetary gearbox torsional vibration effects on wound-rotor induction generator electrical signatures. *IEEE Trans. Ind. Appl.* **2016**, *52*, 4770–4780. [CrossRef]

11.   Marzebali, M.H.; Faiz, J.; Capolino, G.-A.; Kia, S.H.; Henao, H. Planetary gear fault detection based on mechanical torque and stator current signatures of a wound rotor induction generator. *IEEE Trans. Energy Convers.* **2018**, *33*, 1072–1085. [CrossRef]

12.   Bazghandi, R.; Marzebali, M.H.; Abolghasemi, V. Asymmetrical Fault Detection in Induction Motors through Elimination of Load Torque Oscillations Effects in the Slight Speed Variations and Steady-state Conditions. *IEEE J. Emerg. Sel. Top. Ind. Electron.* **2022**, *4*, 725–733. [CrossRef]

13.   Navarro-Navarro, A.; Zamudio-Ramirez, I.; Biot-Monterde, V.; Osornio-Rios, R.A.; Antonino-Daviu, J.A. Current and Stray Flux Combined Analysis for the Automatic Detection of Rotor Faults in Soft-Started Induction Motors. *Energies* **2022**, *15*, 2511. [CrossRef]

14.   Biot-Monterde, V.; Navarro-Navarro, Á.; Antonino-Daviu, J.A.; Razik, H. Stray flux analysis for the detection and severity categorization of rotor failures in induction machines driven by soft-starters. *Energies* **2021**, *14*, 5757. [CrossRef]

15.   Zhukovskiy, Y.; Buldysko, A.; Revin, I. Induction Motor Bearing Fault Diagnosis Based on Singular Value Decomposition of the Stator Current . *Energies* **2023**, *16*, 3303. [CrossRef]

16.   Ye, M.; Zhang, J.; Yang, J. Bearing Fault Diagnosis under Time-Varying Speed and Load Conditions via Observer-Based Load Torque Analysis. *Energies* **2022**, *15*, 3532. [CrossRef]

17.   Benninger, M.; Liebschner, M.; Kreischer, C. Fault Detection of Induction Motors with Combined Modeling-and Machine-Learning-Based Framework. *Energies* **2023**, *16*, 3429. [CrossRef]

18.   Kumar, R.R.; Andriollo, M.; Cirrincione, G.; Cirrincione, M.; Tortella, A. A Comprehensive Review of Conventional and Intelligence-Based Approaches for the Fault Diagnosis and Condition Monitoring of Induction Motors. *Energies* **2022**, *15*, 8938. [CrossRef]

19.   Puche-Panadero, R.; Martinez-Roman, J.; Sapena-Bano, A.; Burriel-Valencia, J. Diagnosis of rotor asymmetries faults in induction machines using the rectified stator current. *IEEE Trans. Energy Convers.* **2019**, *35*, 213–221. [CrossRef]

20.   Ali, H.A.; Elsherbini, M.M.; Ibrahem, M.I. Wavelet Transform Processor Based Surface Acoustic Wave Devices. *Energies* **2022**, *15*, 8986. [CrossRef]

21.   Zhao, Y.; Cui, H.; Huo, H.; Nie, Y. Application of synchrosqueezed wavelet transforms for extraction of the oscillatory parameters of subsynchronous oscillation in power systems. *Energies* **2018**, *16*, 1525. [CrossRef]

22.   Shi, W.; Li, J.; Zhao, B.; Tan, J. An online stress monitoring strategy based on Wigner-Ville time-frequency energy extraction of single-frequency dual mode Lamb waves. *Measurement* **2022**, *200*, 111600. [CrossRef]

23.   Liu, X.; Yan, Y.; Hu, K.; Zhang, S.; Li, H.; Zhang, Z.; Shi, T. Fault diagnosis of rotor broken bar in induction motor based on successive variational mode decomposition. *Energies* **2022**, *15*, 1196. [CrossRef]

24.   Lin, S.-L. Application Combining VMD and ResNet101 in Intelligent Diagnosis of Motor Faults. *Sensors* **2021**, *21*, 6065. [CrossRef]

25.   Tensor Singular Spectrum Decomposition: Multisensor Denoising Algorithm and Application. *IEEE Trans. Instrum. Meas.* **2023**, *72*, 1–15.

26.   Dibaj, A.; Ettefagh, M.M.; Hassannejad, R.; Ehghaghi, M.B. A hybrid fine-tuned VMD and CNN scheme for untrained compound fault diagnosis of rotating machinery with unequal-severity faults. *Expert Syst. Appl.* **2021**, *167*, 114094. [CrossRef]

27.   Wang, C.; Li, H.; Huang, G.; Ou, J. Early fault diagnosis for planetary gearbox based on adaptive parameter optimized VMD and singular kurtosis difference spectrum. *IEEE Access* **2019**, *7*, 31501–31516. [CrossRef]

28.   Zhao, S.; Chen, Y.; Rehman, A.U.; Liang, F.; Wang, S.; Zhao, Y.; Deng, W.; Ma, Y.; Cheng, Y. The inter-turns short circuit fault detection based on external leakage flux sensing and VMD-HHT analytical method for DFIG. In Proceedings of the 2021 International Conference on Sensing, Measurement & Data Analytics in the era of Artificial Intelligence (ICSMD), Nanjing, China, 21–23 October 2021; IEEE: Piscataway Township, NJ, USA, 2021.

29.   Li, H.; Hang, J.; Fang, J.; Zhang, P.; Ding, S.; Wang, Q. Inter-turn fault diagnosis of permanent magnet synchronous machine based on variational mode decomposition. In Proceedings of the 2018 13th IEEE Conference on Industrial Electronics and Applications (ICIEA), Wuhan, China, 31 May–2 June 2018; IEEE: Piscataway Township, NJ, USA, 2018.

30.   Amirat, Y.; Elbouchikhi, E.; Zhou, Z.; Benbouzid, M.; Feld, G. Variational Mode Decomposition-based Notch Filter for Bearing Fault Detection. In Proceedings of the IECON 2019–45th Annual Conference of the IEEE Industrial Electronics Society, Lisbon, Portugal, 14–17 October 2019; Volume 155, pp. 6028–6033.

31.   Li, H.; Liu, T.; Wu, X.; Chen, Q. An optimized vmd method and its applications in bearing fault diagnosis. *Measurement* **2020**, *166*, 108185. [CrossRef]

32.   Puche-Panadero, R.; Pineda-Sanchez, M.; Riera-Guasp, M.; Roger-Folch, J.; Hurtado-Perez, E.; Perez-Cruz, J. Improved resolution of the MCSA method via Hilbert transform, enabling the diagnosis of rotor asymmetries at very low slip. *IEEE Trans. Energy Convers.* **2009**, *24.1*, 52–59. [CrossRef]

33.   Huang, N.E.; Shen, Z.; Long, S.R.; Wu, M.C.; Shih, H.H.; Zheng, Q.; Yen, N.C.; Tung, C.C.; Liu, H.H. The empirical mode decomposition and the Hilbert spectrum for nonlinear and non-stationary time series analysis.*Proc. R. Soc. London Ser. Math. Phys. Eng. Sci.* **1998**, *454*, 903–995. [CrossRef]

34. Grover, C.; Turk, N. Rolling element bearing fault diagnosis using empirical mode decomposition and hjorth parameters. *Procedia Comput. Sci.* **2020**, *167*, 1484–1494. [CrossRef]
35. Korba, K.A.; Arbaoui, F. SVM multi-classification of induction machine's bearings defects using vibratory analysis based on empirical mode decomposition. *Int. J. Appl. Eng. Res.* **2018**, *13*, 6579–6586.
36. Dragomiretskiy, K.; Zosso, D. Variational mode decomposition. *IEEE Trans. Signal Process.* **2013**, *62*, 531–544. [CrossRef]